Controlling the self-doping of epitaxial graphene on SiC via Ar ion treatment

Hae-geun Jee,[1] Kyung-Hwan Jin,[2] Jin-Hee Han,[2] Han-Na Hwang,[1] Seung-Hoon Jhi,[2,*]
Young Dok Kim,[3,*] and Chan-Cuk Hwang[1,*]

[1]*Beamline Research Division, Pohang Accelerator Laboratory, POSTECH, Pohang 790-784, Korea*
[2]*Department of Physics and Division of Advanced Materials Science, POSTECH, Pohang 790-784, Korea*
[3]*Department of Chemistry, Sungkyunkwan University (SKKU), Suwon 440-746, Korea*

(Received 2 April 2011; published 11 August 2011)

We present a simple but efficient way to control substrate-induced doping of graphene via mechanical deformations induced by Ar ions. Graphene on SiC is n-doped because of the substrate-to-graphene charge transfer. Using angle-resolved photoemission spectroscopy (ARPES), core level shift, and scanning tunneling microscopy (STM), the treatment with 0.5-keV Ar ions was found to reduce the charge transfer. First-principles calculations suggest that Stone-Wales defects among various defect structures are likely responsible for the change in the substrate-graphene charge transfer.

DOI: 10.1103/PhysRevB.84.075457 PACS number(s): 71.20.−b, 73.22.Pr

I. INTRODUCTION

Graphene exhibits excellent transparency owing to its single atomic nature, and the Dirac electrons in it move extremely fast with approximately 1/300 of the light velocity, providing a bright prospect of next-generation electronics.[1–3] In order to make various graphene-based devices, control of the doping level in graphene is required. The adsorption of atoms and molecules or the contact with metals have been reported as plausible processes for generating p- or n-type graphene[4–6] by controlling the doping level.

Atomic or molecular doping can be done by the chemisorption of nonmetallic atoms (B, H, O, N)[7–9] or by the adsorption of gas molecules (O_2, H_2O, O_3, NH_3),[10] metals (Li, K, Ca),[11,12] nanoparticles ($AuCl_3$, $FeCl_3$, ZnO),[13] organic molecules (viologen, pyrenebutyrate, isocyanate),[14] or polymers.[15]

The contact of graphene with various substrates is indispensable for graphene growth and the application of graphene to electronic devices. Various metallic (Ru, Ni, Cu, Au, Ag, Pt, Co, Al)[16–18] and nonmetallic (BN)[19] substrates have been reported so far. The electronic property of graphene can be significantly affected by the substrate; for example, the self-doping of graphene by the substrate is commonly observed.

SiC has been a natural choice of substrate for graphene devices since single-layer graphene can be grown epitaxially on it. Graphene is known to become n-doped via electron transfer from the substrate.[20] In this paper we report an efficient way of controlling self-doping of graphene on SiC. When 0.5-keV-Ar ions are irradiated onto monolayer graphene grown on SiC, we find an overall shift of the band structure and the C 1s core-level spectrum toward the Fermi level. This is attributable to the decrease in the charge transfer from the substrate after the ion treatment. First-principles calculations based on density functional theory are utilized to reveal the origin of the change in the substrate-to-graphene charge transfer upon Ar-ion treatment. Among various defect structures considered here, the formation of Stone-Wales (SW) defects is suggested to decrease the work function of graphene, resulting in reduced charge transfer from the substrate. The continuous shift of the electronic levels of graphene upon Ar irradiation suggests that this approach will be easier, more direct, and more applicable than other methods for controlling the electronic nature of supported graphene and thus improving the properties of graphene-based devices.

II. METHODS

A N-doped 6H-SiC(0001) single crystalline wafer with Si termination was cleaned with ethanol in an ultrasonic bath for 15 minutes. The sample was mounted with Ta-clips on a Mo-sample holder and then introduced into an ultrahigh-vacuum preparation chamber. Before single-layer graphene growth, the SiC sample was annealed at 750 °C for degassing and subsequently at 850 °C under Si flux for 30 minutes. The Si flux was produced by direct resistive heating of a Si wafer at approximately 1200 °C. Details of the preparation procedure of single-layer graphene can be found elsewhere.[21–23] The graphene growth was monitored by low-energy electron diffraction, and the thickness of graphene was determined by synchrotron radiation-based photoemission spectroscopy (SRPES) and angle-resolved photoemission spectroscopy (ARPES) at the 7B1 and 3A2 beamlines in Pohang Accelerator Laboratory.[24] Ar^+ ions with 0.5 keV were irradiated onto the single-layer graphene under 1.0×10^{-8} Torr. C 1s core level, and valence-band spectra were taken with photon energies of 340 eV and 55 eV, respectively. Band images of graphene were measured along the direction perpendicular to Γ-K with photon energies of 55 eV and 21.2 eV [ultraviolet (UV) lamp, He I].

In addition to the experiment we carried out first-principles calculations based on the density functional theory. The exchange correlation of electrons was described by the local density approximation, and the projector augmented wave atomic potential was used as implemented in the Vienna Ab-initio Simulation Package (VASP).[25,26] The plane-wave basis set was expanded up to a kinetic-energy cutoff of 400 eV. The convergence of total energy was set to 10^{-5} eV.

III. RESULTS AND DISCUSSION

Figure 1 compares the band images of the pristine and the Ar-ion treated single-layer graphene on SiC, which were taken with He I UV light. As it was previously found, the

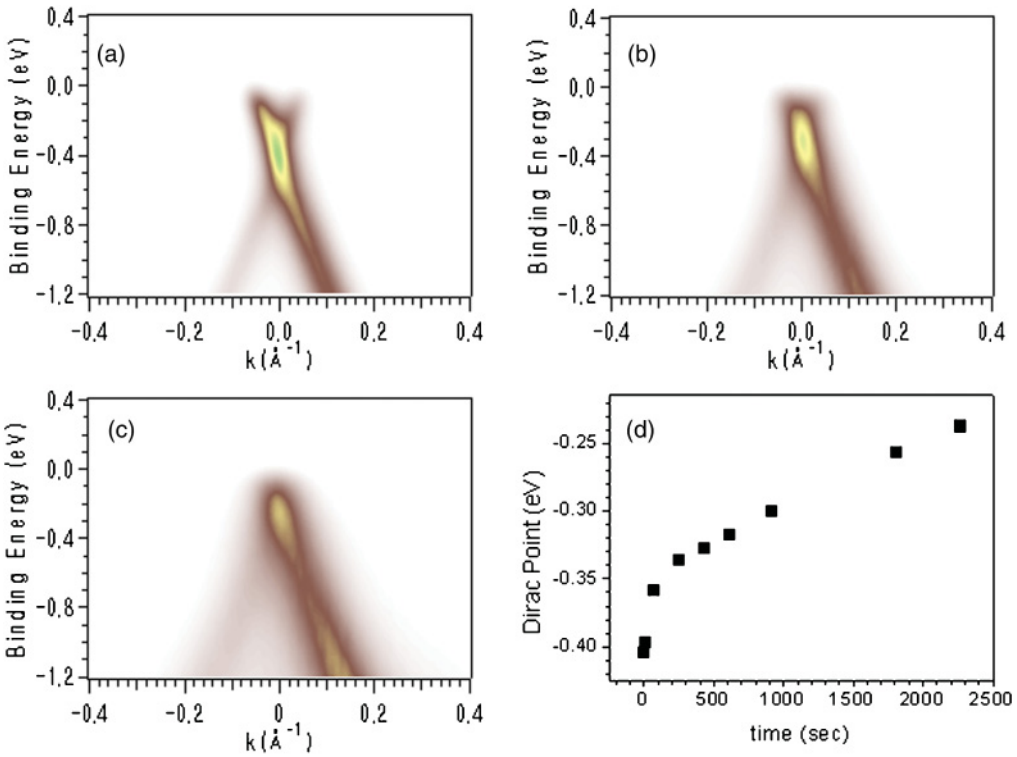

FIG. 1. (Color online) Band images taken by ARPES measurement with a photon energy of 22.1 eV (UV lamp, He I). (a) Image obtained from the pristine graphene. (b) and (c) Images were from Ar-ion irradiated graphene at two different irradiation times, respectively. (d) A plot of Dirac point vs Ar-ion bombardment time. The Dirac point moves up to near-Fermi level after irradiation.

Dirac point of the pristine graphene is located at ∼0.4 eV below the Fermi level, i.e., the graphene layer on SiC is n-doped.[20] This is attributed to a larger work function of graphene than that of SiC, leading to the charge transfer from SiC substrate to graphene layer.[27] We find an upward shift of the band structure by 0.2 eV with respect to pristine graphene layer after graphene was irradiated with Ar ions. This implies that the electron transfer from SiC to graphene become less pronounced after the ion treatment because of the decrease in the work-function difference between graphene and the substrate. If materials with a slightly higher work function than SiC are used as substrate, a lesser n-doped graphene can be formed. The graphene may be changed to a p-type after the ion treatment described previously. Therefore, one would realize p- and n-doped graphene nanostructures, which are the key components of various nanodevices, on a single substrate using selective Ar-ion treatment.

C 1s spectra were also collected before and after bombarding the single graphene layer with Ar ions, as shown in Fig. 2. The C 1s spectra of the surfaces consist of four different components, which can be assigned to the bulk SiC (B), single graphene (G), and buffer (S1 and S2) layers, respectively. After ion bombarding, the C 1s spectrum shifts to lower binding energy by ∼0.2 eV without notable change in the spectral shape and intensity, in line with the whole-band shift toward lower binding energy in Fig. 1 because of the reduced substrate-to-graphene charge transfer.

Scanning tunneling microscopy (STM) was used for studying structural change of graphene created by Ar-ion treatment. We found a flat surface showing a $6\sqrt{3} \times 6\sqrt{3}$R30° superstructure, namely a moiré pattern [Fig. 3(a)]. With a higher resolution a hexagonal structure of the graphene layer can be identified [inset of Fig. 3(a)]. We find lots of protrusions with a diameter of several nanometers after

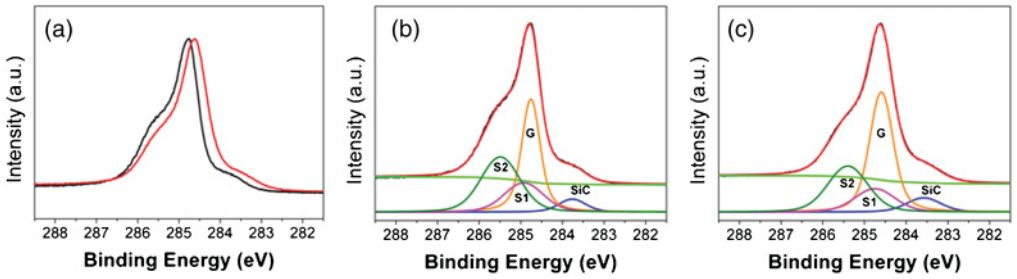

FIG. 2. (Color online) (a) C 1s spectra of the pristine (black) and ion-bombarded (red) single-layer graphene taken with a photon energy of 340 eV. Fitting results of the C 1s spectra of the (b) pristine and (c) ion-bombarded graphene. Blue, orange, pink, and dark green lines correspond to the bulk (SiC), graphene (G), and buffer layers (S1 and S2), respectively.

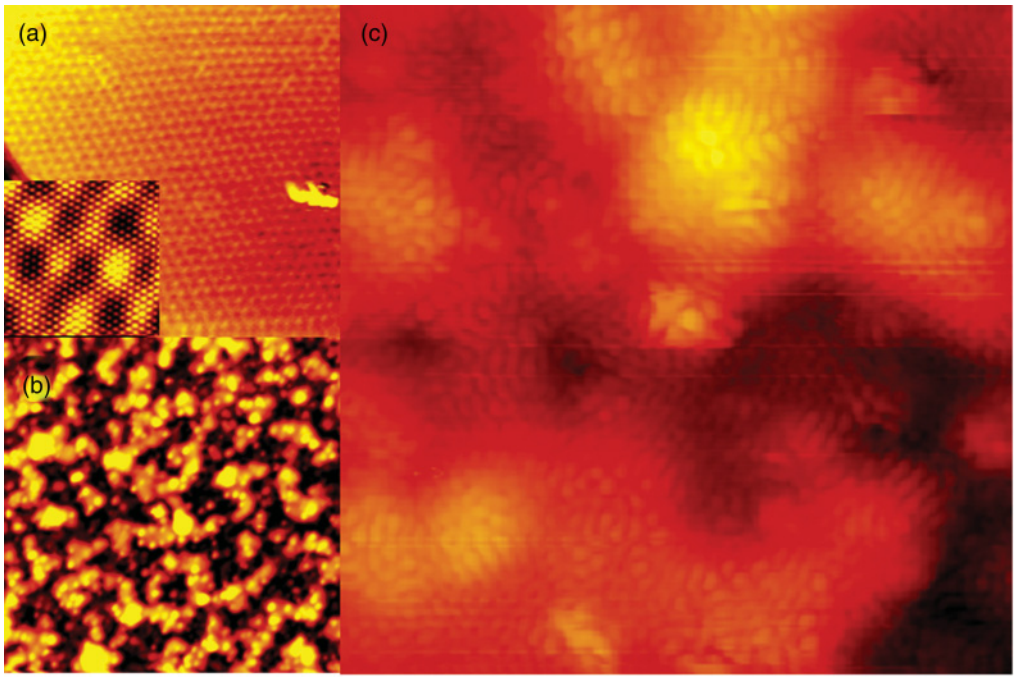

FIG. 3. (Color online) STM images of the pristine (a) and ion-bombarded single-layer graphene at different tunneling conditions (b) and (c). These images were obtained using constant current mode. Image size (a) 500×500 Å^2, (inset) 50×50 Å^2, (b) 500×500 Å^2, and (c) 100×100 Å^2. Tunneling parameters (a) $I_t = 0.13$ nA, $V_t = 940$ mV; (inset) 0.17 nA, 196 mV; (b) 0.15 nA, 490 mV; (c) -0.19 nA, -10.0 mV.

ion bombarding [Fig. 3(b)]. Note that the local hexagonal arrangements corresponding to a $\sqrt{3} \times \sqrt{3}$R30° superstructure can also be identified at most places in the STM image, as shown in the Fig. 3(c). Such an interference pattern has been found at defects.[28] It was difficult in our experiment to know details of the defects created by the Ar-ion treatment because of the interference pattern itself.

In order to investigate what the observed defects are and the origin of the change in the doping level of graphene by Ar-ion treatment, theoretical studies were carried out. We consider here only the change of graphene because Ar ions will change most outer layers the most severely when probed with STM, i.e., one of the most surface-sensitive tools. Because we found no trace of Ar atoms in SRPES after the ion treatment, we can safely neglect some effects of Ar ions imbedded in the sample and discuss only the matter with defects.

As plausible defect structures that may form during the Ar-ion treatment on graphene, we considered the following atomic structures: pristine but winding graphene, SW defect [Fig. 4(a)], 7557-ring structure [Fig. 4(b)], and C2 ad-dimer on graphene. Appropriate supercells are generated to simulate the defect structures. The k-point sampling for the Brillouin-zone integration was done with a $15 \times 15 \times 1$ grid for atomic relaxations and with a $30 \times 30 \times 1$ grid for calculating the work function. The winding graphene was constructed by deforming a supercell of rectangular shape with 6×3-carbon hexagons. The z-axis coordinate (perpendicular to the graphene plane) of the carbon atom at in-plane position (x, y) is shifted by $\Delta z = 0.5 \times \cos(2\pi\lambda x) \times \sin(2\pi\xi y)$, where λ and ξ are the supercell size the x- and y-axis, respectively. The interlayer spacing between layers is 15 Å in z direction for all systems to minimize the artificial-layer interactions.

Table I shows calculated total energies per carbon atom and work function (W) for each defect type to be compared with the pristine case. It was found that all types of defects considered here reduce the cohesive energy. The work function (W) was obtained with respect to the vacuum level, which was set to the saturated electrostatic potential in the region far from graphene planes. Calculated work function for pristine graphene is 4.49 eV, which is consistent with the experimental value of 4.6 eV[29] and other calculations.[30] Only the SW defect between the defect structures shows a reduced work function, which can lower the substrate-to-graphene charge transfer.

The origin of the trend observed in calculated work functions is the strain induced by the defects. Figure 4(e) shows the change in the work function as a function of external strain. As shown in Table I, the C-C bond (averaged over regular carbon hexagons) is shortened in SW defects, which is interpreted as compressive strain. For other defects, on the other hand, the bond length increases and tensile strains are thus induced.

TABLE I. Calculated cohesive energy per carbon atom (E_c), work functions (W, with a change from that of pristine graphene given in parenthesis), and C–C bond length ($d_{C\text{-}C}$) for various types of defects. The $d_{C\text{-}C}$ is the averaged value over regular carbon hexagons around the defect sites.

Type	E_c (eV/atom)	W (eV)	$d_{C\text{-}C}$ (Å)
Pristine graphene	−10.10	4.49	1.413
Winding graphene	−9.98(+0.11)	4.56(+0.07)	1.425
SW graphene	−10.04(+0.06)	4.43(−0.06)	1.406
7557 graphene	−10.02(+0.08)	4.67(+0.18)	1.429
C2 dimer-graphene	−10.00(+0.10)	4.86(+0.37)	1.419

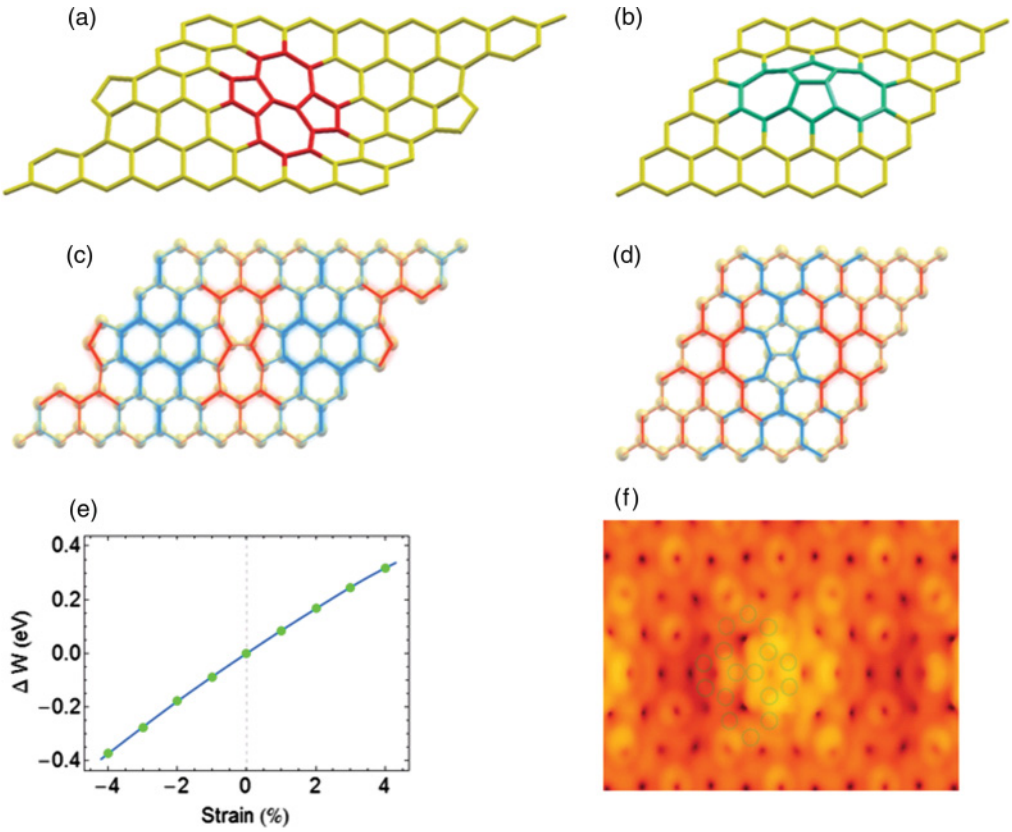

FIG. 4. (Color online) The atomic structure of defective graphenes with (a) SW defect (as depicted in red) and (b) 7557 defect (as depicted in green). Graphic depiction of the change of the C–C bond length in graphene with (c) SW defect and (d) 7557 defect. The red (blue) color indicates the elongation (contractration) of the C–C bond from the normal bond. We observe that the C–C bonds around the SW defect are contracted, while the bonds at only the defect site are elongated. (e) Calculated work-function changes of graphene from the value of pristine graphene at varying (isotropic) strains. Expansion of C–C bonds increases the work function, while the contraction does the opposite. The opposite behavior occurs for 7557 defects. (f) A simulated STM image from a graphene with SW defects.

Figures 4(c) and 4(d) illustrate the change of C-C bonds in graphene with two defect structures. The C-C bond length at the very SW-defect site is increased while the bond length in regular carbon hexagons is decreased. The opposite behavior occurs for graphene with the 7557 defect. Our calculated work functions and formation energies imply that Ar-ion treatment in experiment is likely to generate SW defects. It was pointed out that ripples in graphene can be considered as pseudovector potential,[31] but overall effect is washed out because of their random fluctuation. On the other hand our results demonstrate a robust method of realizing pseudoscalar potential in graphene[32] by sustainable mechanical deformations.

Figure 4(f) shows a simulated STM image from a graphene with SW defects at constant current mode. For simplicity we assumed a free-standing graphene. A voltage range from 0.18 to 0.2 eV was used in accordance with the ARPES and STM data in Figs. 1 and 3(c). In obtaining a single SW-defect image from the supercell calculations, the Brillouin zone of the supercell is unfolded to assign the k-points of a 1×1 phase to the states in this energy range while retaining the amplitude of the wave functions. Note the bright protrusions around the SW defects and the weak $\sqrt{3} \times \sqrt{3}\mathrm{R}30^{\circ}$ pattern, as observed in other defects.[28]

This approach has several advantages over other methods, for example, by molecule adsorption for the alteration of the electronic structure of graphene. First one can keep the highest transparency because no additional layer is introduced in contrast to molecule adsorption. Second the conductivity remains unchanged. We find no considerable change in the slope and the full width at half maximum of momentum distribution curve in the band structure after the ion treatment, indicating that the mobility of the Dirac electrons is not changed.[21] Third this approach is more easily accessible since only an ion source is needed, which is widely available in laboratories. Furthermore by using focused ions one might control the work function in a 5-nm scale.[33] Because of the strong points, we expect our approach could be applicable to a variety of graphene-based devices.

IV. CONCLUSION

In summary we found a decrease in the charge transfer from SiC to graphene by the treatment of 0.5-keV Ar ions as measured by using ARPES, the core-level shift, and STM. Based on first-principles calculations, we suggested that the formation of SW defects by the Ar-ion treatment is related to the reduced substrate-to-graphene charge transfer. Our study showed that the simple ion treatment of graphene can control the doping level of graphene and can be utilized to develop graphene-based electronic devices.

ACKNOWLEDGMENTS

This research was supported by the National Research Foundation of Korea (NRF) funded by the Ministry of Education, Science and Technology (MEST) (Grant Nos. 2009-0083380 and R01-2008-000-20020-0) and by the "Steel Science" project of POSCO. The experiments at Pohang Light Source (PLS) were supported in part by MEST and Pohang University of Science and Technology (POSTECH). K.-H. Jin and S.-H. Jhi were supported by an NRF Grant funded by MEST (No. 2009-0087731) and WCU program No. R31-2008-000-10059-0.

*cchwang@postech.ac.kr, ydkim91@skku.edu, jhish@postech.ac.kr

[1] K. S. Novoselov, A. K. Geim, S. V. Morozov, D. Jiang, M. I. Katsnelson, I. V. Grigorieva, S. V. Dubonos, and A. A. Firsov, Nature **438**, 197 (2005).

[2] Y. Q. Wu, P. D. Ye, M. A. Capano, Y. Xuan, Y. Sui, M. Qi, J. A. Cooper, T. Shen, D. Pandey, G. Prakash, and R. Reifenberger, Appl. Phys. Lett. **92**, 092102 (2008).

[3] K. S. Novoselov, A. K. Geim, S. V. Morozov, D. Jiang, Y. Zhang, S. V. Dubonos, I. V. Grigorieva, and A. A. Firsov, Science **306**, 666 (2004).

[4] W. Chen, S. Chen, D. C. Qi, X. Y. Gao, and A. T. S. Wee, J. Am. Chem. Soc. **129**, 10418 (2007).

[5] X. Wang, X. Li, L. Zhang, Y. Yoon, P. K. Weber, H. Wang, J. Guo, and H. Dai, Science **324**, 768 (2009).

[6] Y.-J. Yu, Y. Zhao, S. Ryu, L. E. Brus, K. S. Kim, and P. Kim, Nano Lett. **9**, 3430 (2009).

[7] U. A. Palnitkar, R. V. Kashid, M. A. More, D. S. Joag, L. S. Panchakarla, and C. N. R. Rao, Appl. Phys. Lett. **97**, 063102 (2010).

[8] R. Faccio, L. Fernández-Werner, H. Pardo, C. Goyenola, O. N. Ventura, and A. W. Mombrú, J. Phys. Chem. C **114**, 18961 (2010).

[9] M. Wu, C. Cao and J. Z. Jiang, Nanotechnology **21**, 505202 (2010).

[10] Z. Liu, X. Lu, P. Peng, W. Wu, S.-S. Pei, Q. Yu, and J. Bao, Phys. Rev. B **82**, 155435 (2010).

[11] Y.-Y. Hu, S.-L. Sun, S. Muhammad, H.-L. Xu, and Z.-M. Su, J. Phys. Chem. C **114**, 19792 (2010).

[12] I. Gierz, C. Riedl, U. Starke, C. R. Ast, and K. Kern, Nano Lett. **8**, 4603 (2008).

[13] K. K. Kim, A. Reina, Y. Shi, H. Park, L.-J. Li, Y. H. Lee, and J. Kong, Nanotechnology **21**, 285205 (2010).

[14] H. K. Jeong, K.-J. Kim, S. M. Kim, and Y. H. Lee, Chem. Phys. Lett. **498**, 168 (2010).

[15] N. Yang, J. Zhai, M. Wan, D. Wang, and L. Jiang, Synthetic Metals **160**, 1617 (2010).

[16] P. W. Sutter, J.-I. Flege, and E. A. Sutter, Nat. Mater. **7**, 406 (2008).

[17] A. Reina, X. Jia, J. Ho, D. Nezich, H. Son, V. Bulovic, M. S. Dresselhaus, and K. Jing, Nano Lett. **9**, 30 (2009).

[18] Gao Li, R. G. Jeffrey, and P. G. Nathan, Nano Lett. **10**, 3512 (2010).

[19] J. Xue, J. Sanchez-Yamagishi, D. Bulmash, P. Jacquod, A. Deshpande, K. Watanabe, T. Taniguchi, P. Jarillo-Herrero, and B. J. LeRoy, Nat. Mater. **10**, 282 (2011).

[20] S. Y. Zhou, G.-H. Gweon, A. V. Fedorov, P. N. First, W. A. de Heer, D.-H. Lee, F. Guinea, A. H. C. Neto, and A. Lanzara, Nat. Mater. **6**, 770 (2007).

[21] H.-G. Jee, J.-H. Han, H.-N. Hwang, B. Kim, H.-S. Kim, Y. D. Kim, and C.-C. Hwang, Appl. Phys. Lett. **95**, 093107 (2009).

[22] C. Berger, Z. Song, T. Li, X. Li, A. Y. Ogbazghi, R. Feng, Z. Dai, A. N. Marchenkov, E. H. Conrad, P. N. First, and W. A. de Heer, J. Phys. Chem. B **108**, 19912 (2004).

[23] E. Rollings, G.-H. Gweon, S. Y. Zhou, B. S. Mun, J. L. McChesney, B. S. Hussain, A. V. Fedorov, P. N. First, W. A. de Heer, and A. Lanzara, J. Phys. Chem. Solids **67**, 2172 (2006).

[24] H.-N. Hwang, H.-S. Kim, B. Kim, C. C. Hwang, S. W. Moon, S. M. Chung, C. Jeon, C.-Y. Park, K. H. Chae, and W. K. Choi, Nucl. Instrum. Meth. A **581**, 850 (2007).

[25] G. Kresse and J. Hafner, Phys. Rev. B **47**, 558 (1993).

[26] G. Kresse and J. Furthmüller, Phys. Rev. B **54**, 11169 (1996).

[27] S. Kopylov, A. Tzalenchuk, S. Kubatkin, and V. I. Fal'Ko, Appl. Phys. Lett. **97**, 112109 (2010).

[28] G. M. Rutter, J. N. Crain, N. P. Guisinger, T. Li, P. N. First, and J. A. Stroscio, Science **317**, 219 (2007).

[29] C. Oshima and A. Nagashima, J. Phys.: Condens. Matter **9**, 1 (1997).

[30] G. Giovannetti, P. A. Khomyakov, G. Brocks, V. M. Karpan, J. vandenBrink, and P. J. Kelly, Phys. Rev. Lett. **101**, 026803 (2008).

[31] A. Nagashima, N. Tejima, and C. Oshima, Phys. Rev. B **50**, 17487 (1994).

[32] S.-M. Choi, S.-H. Jhi, and Y.-W. Son, Phys. Rev. B **81**, 081407(R) (2010).

[33] [http://www.fei.com/products/focused-ion-beams/v600.aspx], V600 and V600CE Focused Ion Beams, date of access July 26, 2011.